

Millimeter Wave Fuze Radome Design Based Bandpass Frequency Selective Surface

Min Zhao¹, Junjian Bi², Juan Xu^{1,3*}, and Jianping Zhao¹

¹ School of Cyber Science and Engineering, Qufu Normal University, Qufu, 273165, People's Republic of China
zhaomin219@163.com, xujuan125@163.com, zjp-wlx@163.com

² Key Laboratory of Electromagnetic Environmental Effects, Army University of Engineering
Shijiazhuang, 050003, People's Republic of China
13303315178@189.cn

³ State Key Laboratory of Millimeter Waves, Southeast University, Nanjing, 211189, People's Republic of China
*xujuan125@163.com

Abstract — This paper studies a fuze radome system applied to millimeter waves. The system consists of feed antenna, radome, planar FSS array or curve conformal array. Microstrip antenna is used as the feed antenna. Based on the principle of equispaced and equal period respectively, cross units loading single layer dielectric form planar and curve FSS array. The FSS radome system can improve the permeability of hood to electromagnetic waves (EM) of passband, and reduce the interference of complex EM in the external environment to the system. The FSS radome will not deteriorate radiation characteristics of the feed antenna. The planar FSS radome has a passband of 98.2 GHz to 101.55 GHz with -10dB relative bandwidth of 3.35%. The curve FSS radome has a passband of 96.3 GHz to 101.8 GHz with -10dB relative bandwidth of 5.5%. In addition, the radiation characteristics of the proposed system are analyzed. It is found that the radiation pattern of the antenna is basically consistency before and after loading the radome.

Index Terms — Bandpass, frequency selective surfaces, millimeter waves, radiation, radome, transmission.

I. INTRODUCTION

Millimeter waves [1,2] are favored by researchers because of rich frequency resources, small electromagnetic interference in the same frequency band, and narrow beam. FSS radome has a wide application prospect in the fields of electromagnetic protection and reflective surface antennas. Therefore, this paper designs a FSS radome working in the millimeter wave band. The FSS [3-10] is a metal patch or slot unit periodically arranged on the medium, which realizes bandpass or bandstop characteristics by effectively controlling the reflection and transmission characteristics of EM. The

FSS is a spatial filter essentially. The FSS radome not only protects the antenna from the external environment, but also acts as an electromagnetic window to receive and transmit electromagnetic waves of a specific frequency.

In recent years, a large number of studies on frequency selective surfaces have emerged. In [5], the authors proposed an equivalent circuit model of tunable square FSS, which uses discrete capacitive components to achieve tuning, and then approximates the cell size of FSS by circuit model. In [7], a three-dimensional (3D) FSS based on split square coaxial waveguide (SSCW) is proposed, which introduces two transmission zeros on both sides of the passband to achieve high selectivity. In [11], it applies two layers of FSS made of cross element on the radome's dielectric slab. By setting the radome slab thickness as an odd multiple of a quarter-wavelength, the two layers form a phase cancellation structure and suppress electromagnetic wave return. In [12], a filter-antenna consisting of a monopole antenna and a conical FSS radome was designed and investigated. It can keep the input reflection coefficient, radiation pattern of the monopole antenna within the designed passband, and reflects out-of-band signals. The radome [13-18] loaded with bandpass FSS has attracted the attention of many experts and scholars.

The dielectric radome designed in this paper adopts a cone structure. A cross slot unit operating at 100 GHz is used as FSS. A microstrip antenna is used as the feed antenna, because it has stable performance and is easy to integrate with radome. Using the transmission line theory to analyze the influence of different thickness of radome wall on the transmittance, and the influence of various dielectric constant of radome on the radiation performance. It provides reliable theoretical support for improving the radiation performance of FSS radome

system. A planar FSS radome and a curve conformal FSS radome are designed respectively in this paper. The author studied the influence of FSS radome on antenna's S parameters and radiation performance. The numerical results in this article use electromagnetic simulation software HFSS to calculate and solve.

II. TRANSMISSION LINE THEORY AND FULL WAVE ANALYSIS

The equivalent transmission line theory of the radome is used to calculate the transmission coefficient of the radome. The four-terminal equivalent transmission line theory, which is characterized by matrix form, can be applied to radomes of flat structure. For a radome with an N-layer ($N \geq 1$) structure, the transmission characteristics can be represented by a series of N+1 matrices. The radome of the N layers structure is shown in Fig. 1. The relative permittivity and magnetic permeability of air are represented by ϵ_0 and μ_0 , respectively. Similarly, ϵ_i and μ_i show relative permittivity and magnetic permeability of the layer i, and the thickness substrate is represented by d_i .

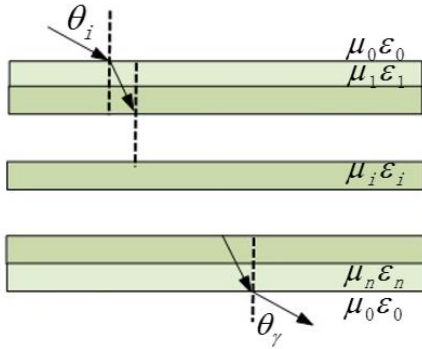


Fig. 1. Schematic of N layers plate electromagnetic wave propagation.

For the structure of the N layers medium, it can be equivalent to an N+1 four-terminal network, and the total cascading matrix T_{all} is expressed as formula (1),

$$T_{all} = \begin{pmatrix} A & B \\ C & D \end{pmatrix} \begin{pmatrix} A_1 & B_1 \\ C_1 & D_1 \end{pmatrix} \begin{pmatrix} A_2 & B_2 \\ C_2 & D_2 \end{pmatrix} \dots \begin{pmatrix} A_n & B_n \\ C_n & D_n \end{pmatrix}, \quad (1)$$

$$\begin{pmatrix} A_i & B_i \\ C_i & D_i \end{pmatrix} = \begin{pmatrix} ch(j\gamma_i d_i) & Z_i sh(j\gamma_i d_i) \\ \frac{sh(j\gamma_i d_i)}{Z_i} & ch(j\gamma_i d_i) \end{pmatrix}, \quad (2)$$

where $\gamma_i = \sqrt{\mu_i \epsilon_i - \sin^2 \theta_i} \times 2\pi / \lambda_0$, $sh()$ and $ch()$ represent hyperbolic sine and hyperbolic cosine functions respectively. The characteristic impedance of the layer i relative to the free space can be normalized to Z_i . The Z_i^{\parallel} represents horizontally polarized normalized characteristic impedance, expressed as formula (3).

The Z_i^{\perp} represents vertical polarization normalized characteristic impedance, expressed as formula (4):

$$Z_i^{\parallel} = Z_0 \frac{\mu_i}{\epsilon_i} \sqrt{\mu_i \epsilon_i - \sin^2 \theta_i}, \quad (3)$$

$$Z_i^{\perp} = \frac{Z_0 \mu_i}{\sqrt{\mu_i \epsilon_i - \sin^2 \theta_i}}, \quad (4)$$

Z_0 in the above equation is the free-space characteristic impedance, $Z_0 = 377\Omega$. For horizontally polarized waves, its characteristic impedance is $Z_0^{\parallel} = Z_0 \cos \theta_0$. For vertically polarized waves, the characteristic impedance is $Z_0^{\perp} = Z_0 / \cos \theta_0$. After solving the total cascading matrix T_{all} of the N four-terminal network, the transmission coefficient can be calculated by the formula (5):

$$Trans = \frac{2}{(A_{all} + B_{all} / Z_0) + (Z_0 C_{all} + D_{all})}. \quad (5)$$

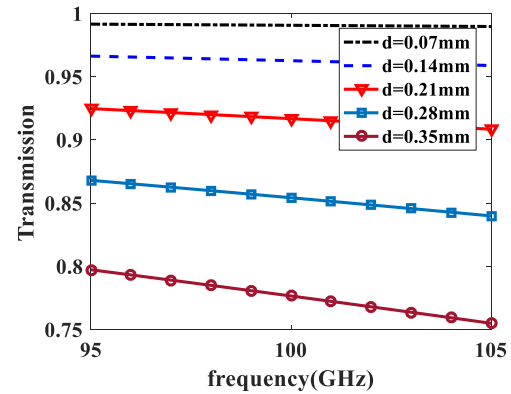


Fig. 2. Effect of radome wall thickness on transmittance.

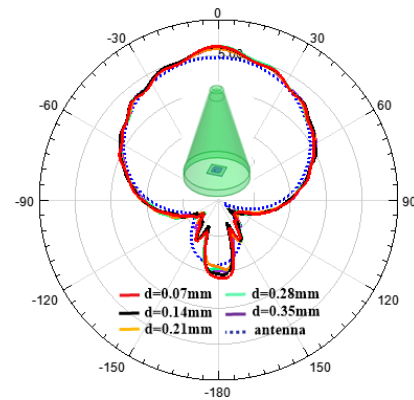


Fig. 3. Effect of radome wall thickness on radiation performances.

Assume that the relative permittivity of radome is 1.08, the transmission rate is decreasing as the thickness increases from 0.07mm to 0.35mm, as shown in Fig. 2.

Table 1 shows the transmission rate at different wall thicknesses at 100 GHz. When the wall thickness is less than or equal to 0.21 mm, the transmission rate is more than 90%. The radiation characteristics of the radome are analyzed in combination with full-wave simulation. Figure 3 shows the effect of the thickness of the radome wall on the radiation performance. In the range of 0.07mm~0.21mm, the radiation curves of different radome wall thicknesses are basically coincident, which is in good agreement with the radiation pattern of the antenna. Combined with the data in Table 1, after loading dielectric radome the gain of antenna is approximately equal to 6dB. In order to ensure the overall strength of the radome, the thickness of the radome is increased as much as possible under the condition that the electrical performance index is satisfied. Therefore, the overall thickness of the radome wall is determined to be 0.21 mm.

Table 1: Comparison of transmission and gain at 100 GHz for different wall thicknesses

d (mm)	0.07	0.14	0.21	0.28	0.35
Trans. (%)	99.06	96.26	91.67	85.42	77.65
Gain (dB)	6.29	6.25	5.99	6.26	6.03

Assume that the thickness of the radome wall is 0.21 mm, the transmission rate decreases with the increase of the relative permittivity of the radome wall, as shown in Fig. 4.

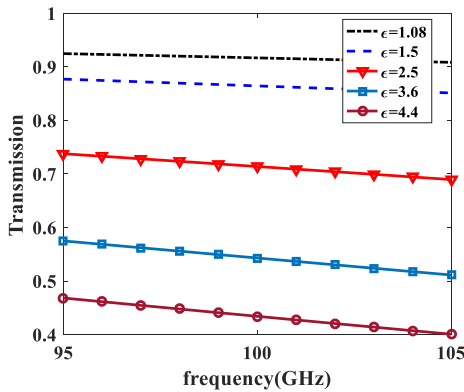


Fig. 4. Effect of permittivity of radome wall on the transmission rate.

Figure 5 shows the effect of relative permittivity of radome wall on the radiation performance. It can be obtained that the radiation pattern is gradually distorted with the increase of the relative permittivity. Table 2 shows the transmission of the different relative permittivity radome at 100 GHz. When the relative permittivity of

radome wall is 1.08, the transmittance is more than 90%. Considering the radiation gain of different wall materials, honeycomb materials with the relative permittivity of 1.08 are selected.

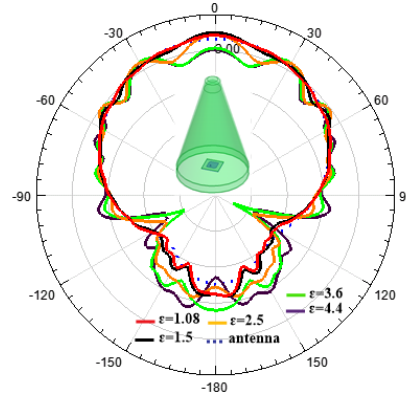


Fig. 5. Effect of relative permittivity of radome wall on radiation performance.

Table 2: Comparison of transmission and gain at 100 GHz for different wall materials

ϵ_r	1.08	1.5	2.5	3.6	4.4
Trans (%)	91.67	86.44	71.39	54.31	43.42
Gain (dB)	5.99	6.52	6.12	5.97	5.44

III. RADOME SYSTEM DESIGN

A. FSS design and simulation

The frequency of FSS depends on the total length of the gap, and resonance occurs when the length is equal to half the wavelength. In this paper, cross slot units are designed for planar and curve FSS radome, as shown in Fig. 6. The planar unit is loaded with Rogers 5880 with dielectric constant of 2.2, and the curve unit is loaded with material with dielectric of 1.08. The size parameters are shown in Table 3.

Table 3: Size parameter of plane and curve cross FSS

Variables	a	D	h	L	w
Plane (mm)	0.07	1.06	0.12	0.37	0.044
Curve (mm)	0.089	1.34	0.152	0.465	0.054

The resonant frequency of the planar and curve unit are 100 GHz, as shown in Fig. 7. When the EM is incident on the radome wall at a large angle, the FSS unit is required to have excellent angle stability. Both units can maintain stable resonance when incidence angle is 0 degrees and 45 degrees by analyzing reflection coefficient and transmission coefficient. It confirms that planar and curve FSS unit have good angle stability.

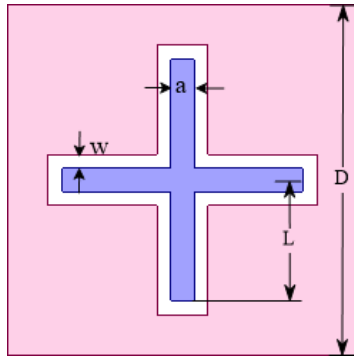


Fig. 6. Classic cross gap type FSS unit.

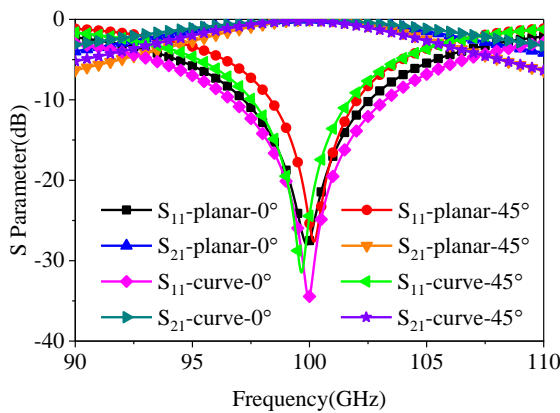


Fig. 7. S parameter of plane and curve FSS unit.

Table 4 analyzes the influence of arm length L on center frequency. As L increases, the center frequency of planar and curve FSS unit both shows downward trend. This further illustrates the inverse relationship between the gap length and center frequency.

Table 4: Effect of the value of w on center frequency

f_0 (GHz)	L (mm)		
		0.32	0.37
Plane	112.8	99.88	86.75
f_0 (GHz)	L (mm)		
		0.45	0.465
Curve	101	99.97	94.68

B. Planar FSS radome design and analysis

Based on requirements for aircraft stability and aerodynamic performance, this paper designs a cone radome. The radome wall adopts a single-layer thin wall to improve the transmission rate. In order to obtain a wider operating frequency band, it is required that the relative permittivity of the material is as low as possible. Meanwhile, the loss of wall material should be as small as possible to improve the transmission efficiency of radome. Figure 8 shows a schematic diagram of the

dielectric radome. Table 5 shows the size parameters of cone radome.

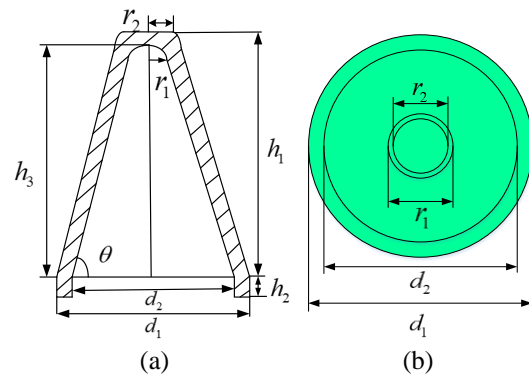


Fig. 8. Schematic diagram of dielectric radome: (a) cross-sectional view and (b) top view.

Table 5: Size parameters of cone radome

Variables	r1	r2	h1	h2
Value (mm)	2.5	3.365	28.64	2.26
Variables	h3	d1	d2	--
Value (mm)	28.14	23.22	20.64	--

The model of planar FSS radome is established through joint programming of HFSS and MATLAB. The author writes programs to call HFSS for automatic modelling using MATLAB's application programming interface (API). Compared with the traditional manual modeling method, this method greatly improves the modeling efficiency and saves time.

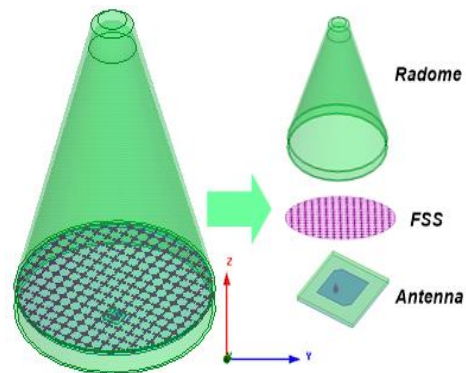


Fig. 9. Planar FSS radome system model.

According to the equidistant principle, the two-dimensional FSS array are arranged along the plane edge of the cylindrical dielectric substrate. Then the planar FSS array are loaded to the bottom of radome. Similarly, the microstrip antenna is placed below the FSS array, and

the planar FSS radome model is shown in Fig. 9. Figure 10 shows the comparison of S_{11} between planar FSS radome system and antenna. The S_{11} curves of the antenna are in good agreement before and after loading planar FSS radome. The absolute bandwidth of the system is 98.2GHz~101.55GHz, and the relative bandwidth is 3.35%. Figure 11 shows the comparison of the E-plane and H-plane radiation characteristics. After loading planar FSS radome, the radiation pattern is shaken slightly. The main lobe gain is basically stable. The beam pointing error is within the allowable range. Figure 12 shows the 3D radiation pattern of dielectric radome, and the gain is approximately 6dB. Figure 13 shows the 3D radiation pattern of planar FSS radome, and the gain is about 6.4dB, which is an increase of 0.4dB compared with loading dielectric radome. It shows that loading the planar FSS radome can increase the radiation gain of the radome system.

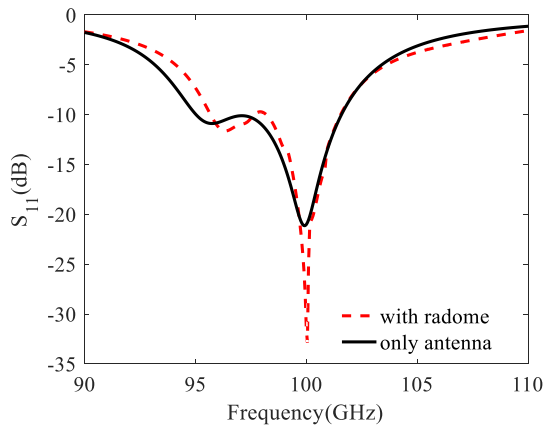


Fig. 10. Comparison of S_{11} between planar FSS radome system and antenna.

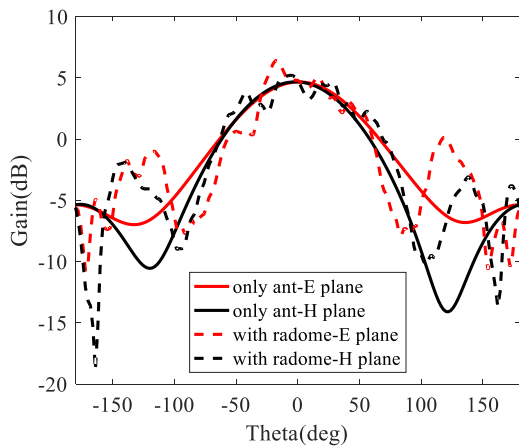


Fig. 11. Comparison of E- and H-plane patterns between planar FSS radome and antenna.

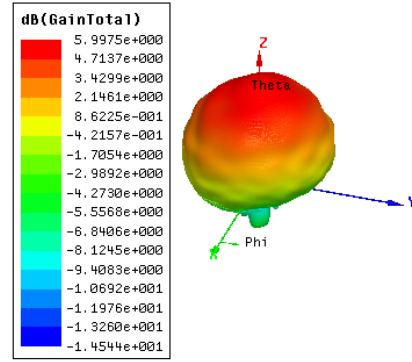


Fig. 12. 3D radiation pattern of substrate radome.

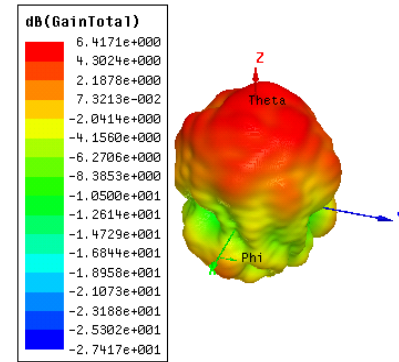


Fig. 13. 3D radiation pattern of planar FSS radome system.

C. Surface conformal FSS design and simulation

Different from planar FSS radome, the FSS array of curve FSS radome is conformal to the surface of cover wall. The modeling method still uses API by calling HFSS automatic modeling in MATLAB programming. According to the principle of quasi-period arrangement, the curve FSS array is composed of classical cross FSS unit. The three-dimensional model of the curve FSS radome system is shown in Fig. 14.

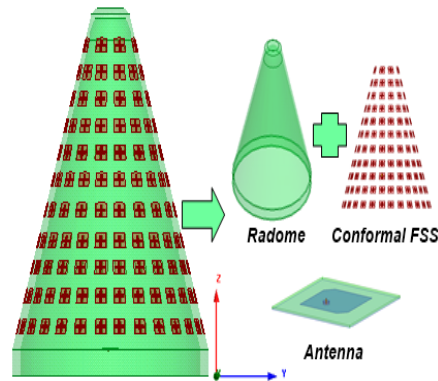


Fig. 14. Curve FSS radome system model.

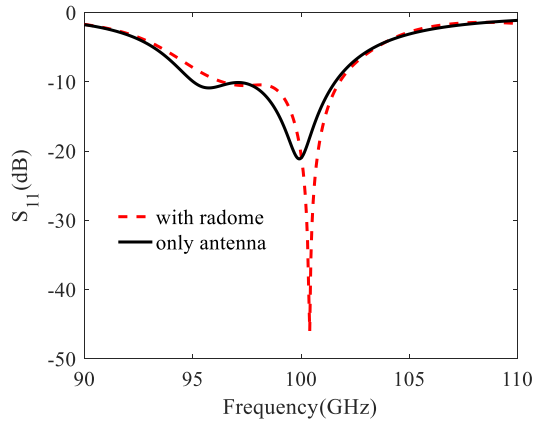


Fig. 15. Comparison of S_{11} between conformal FSS radome and antenna.

The feed antenna uses a microstrip patch antenna, and the center frequency of the radiation is 100 GHz. Figure 15 shows the comparison of S_{11} between curve FSS radome system and antenna. The S_{11} curves of the antenna are in good agreement before and after loading curve FSS radome. The absolute bandwidth of the system is 96.3 GHz to 101.8 GHz. The relative bandwidth is 5.5%. Figure 16 and Fig. 17 show the comparison of the E-plane and H-plane radiation characteristics. Figure 18 shows the 3D radiation pattern of curve FSS radome system. After loading the curve FSS radome, the radiation pattern is dithered slightly compared to the antenna. The main lobe gain is reduced by 1.3 dB, and the beam pointing error is within the allowable range. The backward gain becomes larger and the sidelobe level is raised by 8.17 dB.

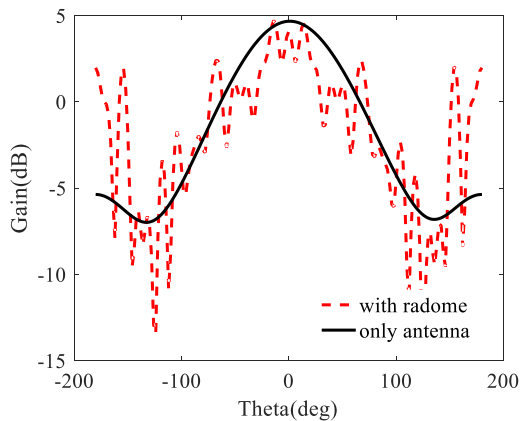


Fig. 16. Comparison of E-plane pattern between curve FSS radome and antenna.

Table 6 has compared the radome structure, frequency band and performance between this paper and literature [12-15]. The FSS radome designed in this

paper is a dome-shaped cone. It works in the millimeter wave band. It has a -10dB bandwidth greater than 3GHz, and the bandwidth in other literatures is less than 2GHz.

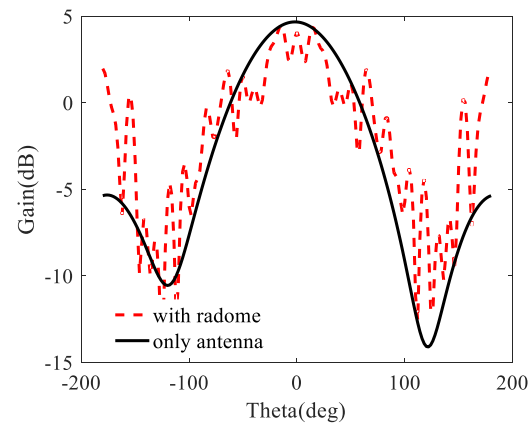


Fig. 17. Comparison of H-plane pattern between curve FSS radome and antenna.

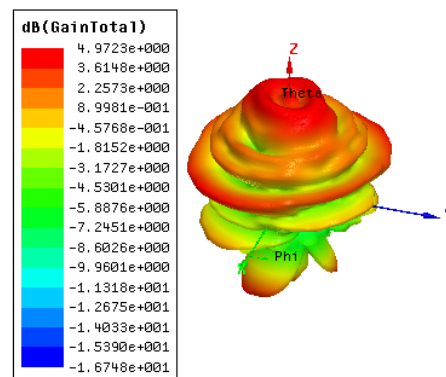


Fig. 18. 3D radiation pattern of curve FSS radome system.

The radome system designed in this paper works in the millimeter wave and the center frequency is 100 GHz. This is extremely demanding for machining accuracy and testing environment. No actual tests have been conducted yet. In the following work, the author will carry out the actual processing based on the data and conclusions obtained in this paper, and then give the comparison results of simulation and actual measurement in the subsequent articles.

IV. CONCLUSION

In this paper, based on the classical cross FSS unit, a planar FSS radome and a curve FSS radome are designed. They can be applied to the front end of the aircraft to prevent electromagnetic interference and improve the permeable performance of radome. The results show that both planar and curve FSS radome

can improve the transmission rate without affecting the radiation characteristics of the antenna. They can suppress interference from out-of-band signals to the system. The

two radome systems designed in this paper have broad application prospects in fuze radomes.

Table 6: Comparison of the proposed structure to the existing structure

Refs.	Frequency (GHz)	Cover Shape	Core Dielectric	FSS Loading	10dB BW (GHz)
[12]	6.1	Conical	2.33	Curved	0.418
[13]	5.3	Flat type	2.55	Planar	0.18
[14]	9.8	Flat type	2.65	Planar	1.5
[15]	12.4	Conical	3	Curved	—
This work	100	Dome cone	1.08	Planar	3.35
		Dome cone	1.08	Curved	5.5

ACKNOWLEDGMENT

This work is funded by Natural Science Foundation of 61701278 and State Key Laboratory of Millimeter Waves Foundation of K201929.

REFERENCES

- [1] D. M. Syahkal and D. Wake, "Bow-tie antennas on high dielectric substrates for MMIC and OEIC applications at millimetre wave frequencies," *Electronics Letters*, vol. 31, no. 24, pp. 2060-2061, Nov. 23, 1995.
- [2] P. Hallbjorner, M. Bergstrom, M. Boman, P. Lindberg, E. Ojefors, and A. Rydberg, "Millimetre-wave switched beam antenna using multiple travelling-wave patch arrays," *IEE Proceedings - Microwaves, Antennas and Propagation*, vol. 152, no. 6, pp. 551-555, Dec. 9, 2005.
- [3] B. Wu, Y.-J. Yang, H.-L. Li, Y.-T. Zhao, C. Fan, and W.-B. Lu, "Low-loss dual-polarized frequency-selective resistor with graphene-based planar resistor," *IEEE Transactions on Antennas and Propagation*, vol. 68, no. 11, pp. 7439-7446, Nov. 2020.
- [4] H. B. Wang, Y. J. Cheng, and Z. N. Chen, "Wideband and wide-angle FSS using loop slotted hybrid quarter-mode substrate integrated cavity with two independently controllable poles," *IEEE Transactions on Antennas and Propagation*, vol. 68, no. 12, pp. 8221-8226, Dec. 2020.
- [5] D. Ferreira, R. F. da Silva Caldeirinha, I. Cuiñas, and T. R. Fernandes, "Tunable square slot FSS EC modelling and optimisation," *IET Microwaves, Antennas & Propagation*, vol. 11, no. 5, pp. 737-742, Apr. 15, 2017.
- [6] F. Costa, A. Monorchio, and G. Manara, "An overview of equivalent circuit modeling techniques of frequency selective surfaces and metasurfaces," *Applied Computational Electromagnetics Society Journal*, vol. 29, no. 12, pp. 960-976, Dec. 2014.
- [7] Z. Yu, X. Yang, W. Tang, Y. Shi, J. Zhu, and C. Wang, "Compact three-dimensional bandpass FSS with high selectivity based on split square coaxial waveguide," *Electronics Letters*, vol. 55, no. 21, pp. 1135-1137, 2019.
- [8] B. Lin, S. Du, H. Zhang, and X. Ye, "Design and simulation of frequency-selective radome together with a monopole antenna," *Applied Computational Electromagnetics Society Journal*, vol. 25, no. 7, pp. 620-625, July 2010.
- [9] A. A. Omar and Z. Shen, "Thin 3-D bandpass frequency-selective structure based on folded substrate for conformal radome applications," *IEEE Transactions on Antennas and Propagation*, vol. 67, no. 1, pp. 282-290, Jan. 2019.
- [10] K. K. Varikuntla and R. Singara Velu, "Design and development of angularly stable and polarisation rotating FSS radome based on substrate-integrated waveguide technology," *IET Microwaves, Antennas & Propagation*, vol. 13, no. 4, pp. 478-484, 2019.
- [11] W.-J. Liao, W.-Y. Zhang, Y.-C. Hou, S.-T. Chen, C. Y. Kuo, and M. Chou, "An FSS-integrated low-RCS radome design," *IEEE Antennas and Wireless Propagation Letters*, vol. 18, no. 10, pp. 2076-2080, Oct. 2019.
- [12] H. Zhou, S. Qu, B. Lin, J. Wang, H. Ma, Z. Xu, W. Peng, and P. Bai, "Filter-antenna consisting of conical FSS radome and monopole antenna," *IEEE Transactions on Antennas and Propagation*, vol. 60, no. 6, pp. 3040-3045, June 2012.
- [13] W. Pan, C. Huang, P. Chen, M. Pu, X. Ma, and X. Luo, "A beam steering horn antenna using active frequency selective surface," *IEEE Transactions on Antennas and Propagation*, vol. 61, no. 12, pp. 6218-6223, Dec. 2013.
- [14] G. Q. Luo, W. Hong, H. J. Tang, J. X. Chen, X. X. Yin, Z. Q. Kuai, and K. Wu, "Filtenna consisting of horn antenna and substrate integrated waveguide cavity FSS," *IEEE Transactions on Antennas and Propagation*, vol. 55, no. 1, pp. 92-98, Jan. 2007.
- [15] Y. W. Chia (Michael), "Radiation from curved (conical) frequency selective surfaces," *Department of Electronic and Electrical Engineering Loughborough University of Technology*, United Kingdom, 1993.
- [16] Y. E. Erdemli, K. Sertel, R. A. Gilbert, D. E. Wright, and J. L. Volakis, "Frequency-selective

surfaces to enhance performance of broad-band reconfigurable arrays,” *IEEE Transactions on Antennas and Propagation*, vol. 50, no. 12, pp. 1716-1724, Dec. 2002.

- [17] B. Munk, *Frequency Selective Surfaces: Theory and Design*. John Wiley & Sons, Inc., 2000.
- [18] H.-Y. Chen and S.-H. Wen, “An empirical formula for resonant frequency shift due to Jerusalem-cross FSS with substrate on one side,” *Applied Computational Electromagnetics Society Journal*, vol. 33, no. 7, pp. 730-740, July 2018.



Min Zhao was born in Dezhou, Shandong Province, China in 1996. She received the B.S. degree in Communication Engineering from QuFu Normal University, Qufu, China, in 2018 and is currently working toward the M.S. degree in Communication and Information Systems at QuFu Normal University. Her research interests include frequency selective surfaces, metamaterials and millimeter wave fields.



Junjian Bi was born in Shijiazhuang, Hebei Province, China, in 1972. He received the Ph.D. degrees in Weapon System and Application Engineering from Beijing University of Technology, Beijing, China, in 2005. At present, he is mainly engaged in the research of electromagnetic environment effect technology of equipment.



Juan Xu was born in Jining, Shandong Province, China, in 1982. She received the Ph.D. degrees in Electronic Science and Technology from Nanjing University of Science and Technology, Nanjing, China, in 2016. Since 2016, she has worked at QuFu Normal University. She has been an associate professor since 2019.

Her research interests include simulation, design and experimental measurement of new high performance RF, microwave and millimeter wave passive devices, antennas and antenna arrays.



Jianping Zhao was born in Heze, Shandong Province, China, in 1964. He received the B.S. degree in Physics from QuFu Normal University, Qufu, China, in 1985. In 1988, he studied in Wuhan University for master's degree in Radio and Information Engineering.

Since 1985, he has worked at QuFu Normal University. He was promoted to Associate Professor in 1997, Professor in 2002. Since 1992, he has been the Director of the Radio Teaching and Research Section. He has been engaged in application of electronic technology and scientific research in communication and information system of electronic information engineering and communication engineering.